ASTRONOMY & ASTROPHYSICS
SUPPLEMENT SERIES

JANUARY I **2000**, PAGE 65

Astron. Astrophys. Suppl. Ser. **141**, 65–77 (2000)

A representative sample of Be stars

II. *K* band spectroscopy

J.S. Clark[1] **and I.A. Steele**[2]

[1] Astronomy Centre, CPES, University of Sussex, Brighton, BN1 9QH, UK
[2] Astrophysics Research Institute, Liverpool John Moores University, Liverpool, L41 1LD, UK

Received February 16; accepted September 29, 1999

Abstract. We present K band ($2.05\ \mu\mathrm{m} - 2.22\ \mu\mathrm{m}$) spectra of 66 isolated Be stars of spectral types O9-B9 and luminosity classes III, IV & V. We find that objects with He I features either in emission or absorption are B3 or earlier. Objects with Mg II emission but no He I are B2 to B4, while objects with Brγ emission but no evidence of He I or Mg II are B5 or later. Na I emission in the spectra of 4 objects appears to indicate that regions of the circumstellar envelopes of these stars must be shielded from direct stellar radiation. Systematic trends in the line strength and profile of Brγ are seen from early to late spectral types which can be understood in terms of differences in the disc temperature and density. 30 per-cent of the stars do not currently show evidence for line emission. Compared to the emission line stars these objects have a significantly lower mean rotational velocity and a distribution of spectral types that is significantly earlier. This can be explained either as the original misidentification of these objects as Be stars (i.e. they never had line emission), or as evidence that stars with lower rotational velocities may be more prone to changes between the Be and B phases.

Key words: stars: emission-line, Be — infrared: stars

1. Introduction

Classical Be stars are non-supergiant B stars which show, or have shown, Balmer line emission. In addition they show an infra-red continuum excess due to free free and bound free emission from a dense circumstellar envelope. Comparison of optical and UV spectra reveals the presence of a second circumstellar wind regime; a lower density, high velocity polar component responsible for the high excitation lines visible in UV spectra. That the denser component was concentrated in the equatorial plane has long been suspected. Recent interferometric data has confirmed this hypothesis (Quirrenbach et al. 1994; Stee et al. 1995).

Despite these direct observations of the circumstellar envelope, the dynamics and physical conditions within it are still largely unconstrained. Determination of parameters such as the density and temperature gradient of the disc would allow constraints to be placed on theoretical models of the Be phenomenon. At present some success has been achieved by modeling the continuum excess and Hα line profile (Waters 1986; van Kerkwijk et al. 1995). However, the optical Hydrogen transitions do not allow us to probe the inner regions of the circumstellar disc. The rich recombination spectrum of Be stars in the near–IR provides a powerful tool to address these problems, given that the lines present at these wavelengths are likely to originate at smaller disc radii than those present in the optical region. Therefore, we can use near–IR spectra to probe the inner regions of the circumstellar disc where it is possible that deviations from a quasi–Keplerian disc may occur, due to transport of angular momentum, for example. Additionally, given that near IR wavelengths are less affected by interstellar extinction, it is hoped that a spectral classification scheme for classical Be stars can be developed for use in situations where standard optical classification is inappropriate (such as the identification of highly reddened counterparts to X-ray transient systems where it is impossible to obtain optical spectra for classification purposes).

This paper is the second of a series on the optical and near IR spectral properties of a representative sample of Be stars. In Steele et al. (1999) (Paper I) we presented optical spectra of a sample of 58 Be stars. The sample contains objects from O9 to B8.5 and of luminosity classes III (giants) to V (dwarfs), as well as three shell

Send offprint requests to: J.S. Clark
Correspondence to: jsc@star.cpes.susx.ac.uk

stars.

A spectral type and value of $v \sin i$ was derived for each object in the sample. The sample is termed a "representative" sample, in that it was selected in an attempt to contain several objects that were typical of each spectral and luminosity class in the above range. It therefore does *not* reflect the spectral and luminosity class space distribution of Be stars, but only the average properties of each subclass in temperature and luminosity. The distribution of $v \sin i$ within each temperature and luminosity class was carefully investigated and the conclusion drawn that there were no significant selection effects biasing the average properties of the objects.

This paper (Paper II) presents K band ($2.05-2.22\,\mu$m) spectra of the 58 stars from Paper I, plus eight additional objects (Tables 1 and 2). The spectra show H I, He I and various metallic transitions. This paper discusses the relationships between the properties of the underlying B stars in the sample (from Paper I) with those of the observed transitions. Future papers in this series will extend this approach to the emission features present in optical, near-infrared and infra-red H band spectra of the same sample, with the eventual intention of modelling the combined datasets.

2. Observations and data reduction

This paper describes results obtained with the Cooled Grating Spectrometer (CGS4) of the United Kingdom Infrared Telescope (UKIRT), Mauna Kea, Hawaii. The observations were carried out during the periods of 1996 June 28 - 29 and 1996 September 30 - October 2 (see Tables 1 and 2). CGS4 provides spectral coverage from 1 to 5 μm and the observations described here were made using the 256×256 pixel infrared array as a detector. The observations were made using the short focal length camera plus the 150 line/mm grating, giving coverage from 2.05 to 2.22 μm with a velocity resolution of ~ 70 km s^{-1}.

Initial data reduction was carried out at the telescope using the CGS4DR software (Puxley et al. 1992). This removes bad pixels, debiases, flat-fields, linearity corrects and interleaves oversampled scan positions. The subsequent stages of data reduction were carried out using the Starlink-supported package FIGARO. For each target and standard this comprised correcting slit rotation, sky subtraction, extraction, derippling and wavelength calibration using observations of a CuAr lamp.

In order to ensure accurate removal of telluric features from the spectra we followed a procedure similar to that outlined by Hanson et al. (1996, henceforth HCR96). An A0 - A3 III-V star was observed after each target at an airmass within 0.1 of the target. Once per hour observations were also taken of a G2-3V star. The only non-telluric feature in the A star spectra is Brγ. A simple interpolation over this feature is not appropriate however, as there is also a telluric feature at this wavelength that would lead to spurious emission features contaminating the strength and profile of the Brγ emission lines we expect from our targets. Instead we used the G star observations divided by the solar spectrum to calculate the telluric features in the region of Brγ. These were then patched into the A star spectra. Note that in order to ensure the A star, G star, target and solar spectra were all properly aligned in wavelength space cross correlations of various telluric and stellar photospheric features were derived for each spectrum and the appropriate offsets applied.

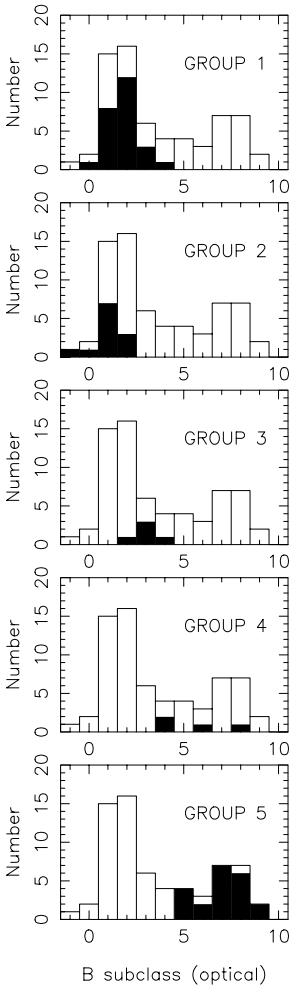

Fig. 1. Histograms showing the membership of each of the spectral groupings by spectral type (solid areas). The distribution of spectral types for the total data set is also indicated on each plot (hollow areas). The data have been binned into n bins containing objects in the range B(n-1).5 to B(n).4. Therefore a B0.2 object will appear in the B0 bin, however a B0.5 object appears in the B1 bin

3. Results and general spectral morphology

The spectral range employed ($2.05 - 2.22$ μm) was chosen due to the large number of transitions of differing

Table 1. Summary of the stellar parameters of the program stars (I). The spectral classifications and values of $v \sin i$ are from Paper I. Those values in italics are taken from the literature. $w \sin i$ is the projected breakup velocity of the star; see Sect. 5 for a further description. The morphological classification of each spectrum according to the criteria listed in Sect. 3 is listed in Col. 6, and the date of each observation (in 1996) in Col. 7

Object name	Aliases	Spectral Type	$v \sin i$	$\omega \sin i$	Group	Date
CD−28 14778	HD 171757	B2III	153 ± 21	0.42	1	29/06
CD−27 11872	V3892 Sgr, HD 161103	B0.5V-III	224 ± 33	0.48	1	29/06
CD−27 13183	HD 172158	B7V	174 ± 10	0.43	5	29/06
CD−27 16010	ϵ PsA, HR 8628, HD 214748	B8IV	187 ± 32	0.54	5	28/06
CD−25 12642	HD 164741	B0.7III	77 ± 18	0.19	2	29/06
BD−20 05381	HD 177015	B5V	202 ± 10	0.45	5	28/06
BD−19 05036	V3508 Sgr, HD 170682	B4III	121 ± 10	0.32	4	29/06
BD−13 00893	DU Eri, HR 1423, HD 28497	*B1-3V*	*270*	*0.57*	1	30/09
BD−12 05132	HD 172252	BN0.2III	120 ± 43	0.29	1	29/06
BD−08 00929	HD 30076	*B2V*	-	-	3	30/09
BD−05 01710	HR 2418, HD 47054	*B8V*	*210*	0.52	5	02/10
BD−02 05328	HD 196712	B7V	151 ± 15	0.35	5	28/06
BD−01 03834	HD 187350	B2IV	168 ± 34	0.41	1	28/06
BD−00 01468	HD 50209	*B9V*	-	-	5	02/10
BD−00 03543	HD 173371	B7V	271 ± 54	0.66	5	29/06
BD+00 01203	HD 39447	*B5III*	-	-	5	01/10
BD+01 01005	ψ01 Ori, HR 1789, HD 35439	*B1-3V*	-	-	1	01/10
BD+02 03815	HD 179343	B7-8sh	224 ± 14	0.62	5	28/06
BD+04 01002	47 Ori, HR 1934, HD 37490	*B2-3III*	*155*	*0.33*	1	01/10
BD+05 03704	HD 168797	B2.5V	221 ± 10	0.47	1	29/09
BD+17 04087	HD 350559	B6III-V	156 ± 39	0.42	4	28/09
BD+19 00578	13 Tau, HR 1126, HD 23016	B8V	240 ± 70	0.59	4	30/09
BD+20 04449	HD 191531	B0III	81 ± 11	0.19	2	28/06
BD+21 04695	25 Peg, HD 210129	B6III-V	146 ± 10	0.40	5	28/06
BD+23 01148	HD 250289	B2III	101 ± 10	0.28	2	02/10
BD+25 04083	HD 339483	B0.7III-B1II	79 ± 11	0.20	2	28/06
BD+27 00797	HD 244894	B0.5V	148 ± 74	0.27	2	01/10
BD+27 00850	HD 246878	B1.5IV	112 ± 25	0.26	2	02/10
BD+27 03411	β2 Cyg, HR 7418, HD 183914	B8V	194 ± 10	0.56	5	28/06
BD+28 03598	HD 333452	O9II	90 ± 12	0.21	2	28/06
BD+29 03842	HD 33226	B1II	91 ± 16	0.23	2	28/06
BD+29 04453	HD 205618	B1.5V	317 ± 20	0.63	1	28/06
BD+30 03227	HR 6971, HD 171406	B4V	218 ± 21	0.48	4	29/06
BD+31 04018	V2113 Cyg, HD 193009	B1.5V	211 ± 11	0.42	1	29/06
BD+36 03946	HD 228438	B1V	186 ± 21	0.36	1	28/06
BD+37 00675	HR 894, HD 18552	B7V	207 ± 29	0.48	5	30/09
BD+37 03856	HD 228650	B0.5V	104 ± 17	0.19	2	28/06
BD+40 01213	HD 33604	B2.5IV	128 ± 20	0.32	1	02/10
BD+42 01376	V434 Aur, HD 37657	B2V	196 ± 10	0.41	1	02/10
BD+42 04538	HD 216581	B2.5V	282 ± 10	0.6	3	28/06
BD+43 01048	HD 276738	B6IIIsh	220 ± 20	0.67	5	30/09
BD+45 00933	HD 27846	B1.5V	148 ± 16	0.29	2	30/09
BD+45 03879	HD 211835	B1.5V	193 ± 10	0.38	1	28/06
BD+46 00275	ϕ And, HR 335, HD 6811	B5III	113 ± 21	0.33	5	30/06
BD+47 00183	22 Cas, HR 193, HD 4180	B2.5V	173 ± 12	0.36	3	30/09
BD+47 00857	ψ Per, HR 1087, HD 22192	B4IV-V	212 ± 16	0.47	3	30/09
BD+47 00939	48 Per, HR 1273, HD 25940	B2.5V	163 ± 12	0.35	3	30/09
BD+47 03985	EW Lac, HR 8731, HD 217050	B1-2sh	284 ± 20	0.67	1	28/06
BD+49 00614	HD 13867	B5III	90 ± 27	0.27	5	30/09

Table 2. Summary of the stellar parameters of the program stars (II). Notation as Table 1

Object name	Aliases	Spectral Type	$v \sin i$	$w \sin i$	Group	Date
BD+50 00825	HR 1160, HD 23552	B7V	187 ± 10	0.44	5	30/09
BD+50 03430	HD 207232	B8V	230 ± 15	0.56	5	28/06
BD+51 03091	HR 8259, HD 20551	B7III	106 ± 10	0.33	5	28/06
BD+53 02599	HD 203356	B8V	191 ± 23	0.47	5	28/06
BD+55 00552	HD 13669	B4V	292 ± 17	0.65	1	30/09
BD+55 00605	V361 Per, HD 14605	B1V	126 ± 35	0.25	1	30/09
BD+55 02411	HD 195554	B8.5V	159 ± 90	0.39	5	29/06
BD+56 00469	V473 Per, HD 13831	*B0-2III*	167 ± 28	0.33	1	30/09
BD+56 00473	V356 Per	B1V-III	238 ± 19	0.54	1	30/09
BD+56 00478	V358 Per, HD 13890	B1.5V	157 ± 12	0.31	1	30/09
BD+56 00484	V502 Per	B1V	173 ± 16	0.33	1	30/09
BD+56 00493	-	B1V-IV	270 ± 10	0.52	2	30/09
BD+56 00511	-	B1III	99 ± 14	0.25	1	30/09
BD+56 00573	-	B1.5V	250 ± 58	0.5	1	30/09
BD+57 00681	HD 237056	B0.5V	147 ± 49	0.27	1	30/09
BD+58 00554	HD 237060	B7V	229 ± 10	0.54	5	30/09
BD+58 02320	HD 239758	B2V	243 ± 20	0.51	1	28/06

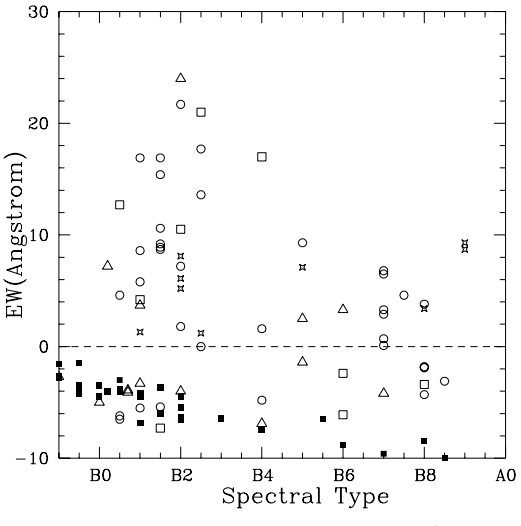

Fig. 2. Plot of Brγ equivalent width (EW) in -Å against spectral type. Triangular symbols represent luminosity class III, squares luminosity class IV and circles luminosity class V. Star symbols represent those objects with only a historical classification. Filled squares represent data for normal B III-V stars taken from HCR96

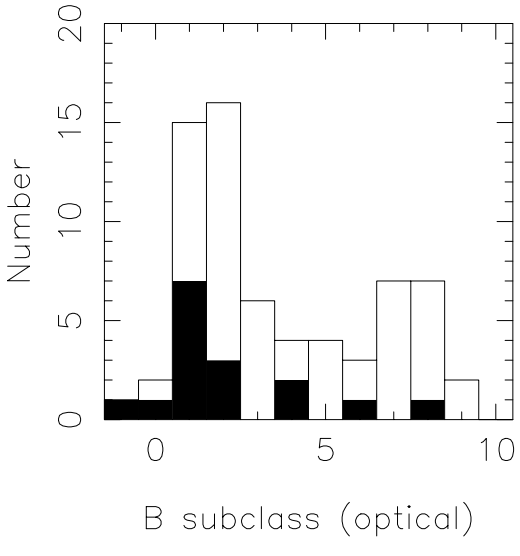

Fig. 3. Histogram showing the number of stars which have undergone a phase change (solid areas) and the total distribution of stars as a function of spectral type (hollow plus solid areas)

species present. Expected transitions within the range include Brγ at 2.166 μm and He I transitions at 2.058 μm, 2.112/2.113 μm and 2.161 μm. Various metallic transitions expected include Fe II 2.089 μm, Mg II 2.138/ 2.144 μm and Na I 2.206/ 2.209 μm. Several transitions of higher excitation species such as He II, C IV and N III are also present in the observed range. However we do not expect to see these given the relatively low temperature expected for the circumstellar envelope of Be stars (e.g. McGregor et al. 1988; Morris et al. 1996).

We present the spectra in Figs. 7–12. Since one of the aims of this work was to derive a K band spectral classification scheme, we have chosen to display the spectra based on their morphology rather than optical spectral classification. We define 5 groups for the spectra, based on the presence and strength of the Brγ, Mg II and He I features; we list the selection criteria below.

Group1: Brγ in emission and He I features present.
Group2: Br γ in absorption and He I features present.
Group3: Brγ & Mg II in emission, no evidence for He I features.
Group4: Brγ in absorption, no evidence for He I or Mg II features.
Group5: Brγ in emission, no evidence for He I or Mg II features.

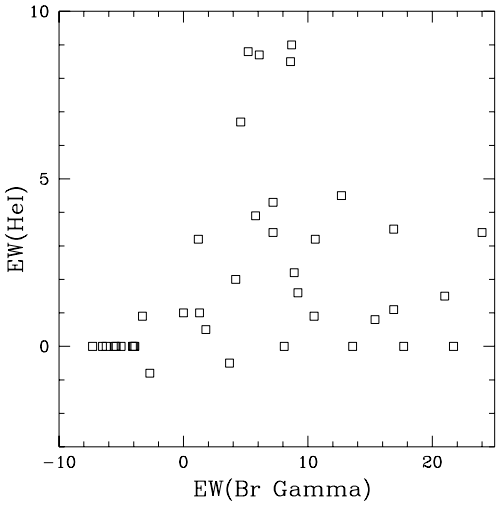

Fig. 4. Plot of Brγ equivalent width (EW) in $-$Å against He I 2.058 μm (EW)

In Fig. 1 we plot the membership of each group by spectral type, and find that this provides a good indication of the broad optical spectral classification of a given star (the small number of non main sequence objects precludes comment on luminosity class). The presence of He I features in either emission or absorption indicates a spectral type of B3 or earlier. The small number of stars that show Mg II in emission, but no evidence of He I features are found to be slightly later (B2-B4), while those stars with Brγ in emission, but which show no evidence of He I or Mg II features are found to be of spectral type B5 or later. Note we chose not to classify stars on the basis of line profiles so that the scheme is applicable to stars for which only low resolution spectra are available.

We summarise the various emission features observed as a function of spectral type in Table 3 (only those stars with classifications given in Paper I are listed). In Tables 4 to 8 we present the measured equivalent widths (EW) of the emission and absorption line features present in each object. These were measured relative to a continuum defined using the interactive routine ABLINE in FIGARO.

4. Relations between emission line strengths and spectral class

4.1. Brackett γ

Brγ is observed in emission in 70 per cent of the stars in the sample. Previous observations of optical H I transitions (e.g. Zorec & Briot 1997) suggest a strong correlation between line strength and stellar temperature; we plot the EW of Brγ against the spectral type of the star in Fig. 2. Although a strong linear correlation between spectral type and EW is not present, a general trend of stronger emission from stars of an early spectral type is evident, with no star of spectral type later than B4 having an $EW_{Br\gamma}$ >10 Å[1].

There appears to be no correlation between $EW_{Br\gamma}$ and luminosity class of the object, although this may be a result of the relatively small number of non main sequence stars observed.

The general trend of stronger Brγ emission at earlier spectral types can be understood in the light of the simulations of the infrared spectrum of ψ Per (Marlborough et al. 1997; henceforth MZW97). They show that the strength of Brγ is very sensitive to both the changes in disc density and temperature (and the radial gradients of these parameters). For the near infrared Hydrogen lines a decrease in disc temperature in general leads to a decrease in line emission for two reasons. Firstly, the source function of the line (taken to be the Planck function; MZW97) decreases with the disc temperature. Also, the temperature dependant factors in the disc opacity term (Eq. (5) of MZW97) cause the opacity to increase with decreasing temperature for the majority of the disc (see Sect. 6.1). Therefore both effects combine to reduce the line emission from the disc as the temperature decreases. Since the disc temperature is likely to be a function of stellar temperature a reduction in line emission from early to late stars is expected.

A decrease in disc density also leads to a decrease in the strength of the IR emission lines (MZW97). The scatter in Fig. 2 could arise from differences in disc density (or density gradient) between individual stars, although we note that a dependance of disc density (and hence line emission) on spectral type is also possible if the disc formation mechanism is dependant on radiation pressure in some manner.

The stars from groups 2 & 4 (with Brγ in absorption) can clearly be distinguished, with the EW of the photospheric profiles being ∼equal to those seen for non emission B stars of the same spectral type (HCR96). The same is found for the strengths of the He I 2.058 and 2.112 μm features of the stars in Group 2. On this basis, despite their prior classification as Be stars we find nothing to distinguish them from field B stars. This raises two possibilities. Firstly it may be that these objects were simply originally misclassified. The second possibility is that since the Be phenomenon is known to be variable, it may simply mean that these particular objects have undergone a phase change from emission ("e") to non-emission ("non-e"). However in Fig. 3 we plot the distribution of these stars against spectral type. Comparing the distributions of "non-e" (groups 2 & 5) and "e" stars with a Kolmogorov-Smirnov (KS) test we find that the the distributions differ at the 3σ level. This could imply that these objects are *not* Be stars in a "non-e" phase. We will return to this question in Sect. 5.

[1] Note that in this paper we will employ the convention that *positive* equivalent widths indicate *emission* features.

Table 3. Summary of the total number of stars by spectral type showing a particular line in emission for which an EW is measurable. Numbers in brackets refer to the number of stars for which the line is seen in emission, but no measurement of EW is possible (those stars designated as *em* in Tables 4–8). Only those stars with spectral classifications made in Paper I are listed

Spec. type	No. stars	Brγ	He I 2.058	He I 2.112	He I 2.161	Mg II	Fe II	Na I
B0	2	1	1	0	0 (1)	0 (1)	0	0 (1)
B0.5	5	2	2 (1)	1	0 (1)	1	0	0 (1)
B1	9	6	5	1	0 (1)	3	1	0
B1.5	8	6	6	0	0 (1)	3	4	0 (1)
B2	5	4	4	0	0 (1)	3	0	0
B2.5	5	5	1	0	0	4	3	0 (1)
B4	4	2	0	0	0	0 (1)	1	0
B5	3	2	0	0	0	0	2	0
B6	3	2	0	0	0	0	1	0
B7	6	6	0	0	0	0	2	0
B8	6	5	0	0	0	0	0	0
B8.5	1	1	0	0	0	0	0	0
B9	1	1	0	0	0	0	0	0
Total	58	43	19 (1)	2	0 (5)	14 (2)	14	0 (4)

4.2. Helium I

He I 2.058 μm emission is confined to the early stars of the sample; being seen in 19 of the 34 stars with spectral types determined in Paper I to be earlier than B2.5 (the dual requirements of a large ionising flux and a dense circumstellar environment required to drive He I 2.058 μm into emission are likely to be present only in the earliest stars). The relative strength of the He I 2.058 μm transition is due to the fact that the disc density falls off more rapidly with radius than the stellar radiation density, enabling the disc to remain ionised to large radii. Primarily populated by recombination, He I 2.112 μm is also only expected to be in emission in the earliest stars, and indeed is only seen in Bd+55 605 (B1V) and Bd+57 681 (B0.5V); in previous studies of hot emission line objects (e.g. Morris et al. 1996) this was absent from all B stars with the exception of the B[e] star S–18. Weak He I 2.161 μm emission is observed in 3 stars, with possible detections in a further 3, all with a spectral type of B2 or earlier (see Table 4).

We plot the Brγ and He I 2.058 μm EW's for those stars of spectral type B2.5 and earlier in Fig. 4, and find that no linear correlation exists between the two quantities. This lack of correlation is likely due to the extreme sensitivity of the He I 2.058 μm line to changes in the UV continuum and optical depth. Consequently, beyond being used as an indicator of early (<B2.5) spectral type, this transition is a poor diagnostic for spectral classification. We find that $EW_{HeI} > EW_{Br\gamma}$ for only three stars out of the 22 stars with both He I 2.058 μm and Brγ in emission. Unfortunately none of the stars were re-examined in Paper I and so only the historical classification of B1–3V is available. We note that in the K band spectra of the Be X-ray binaries (Clark et al. 1999) all of the systems with both Brγ and He I 2.058 μm in emission showed a line ratio in excess of unity; whether this represents a modification of their circumstellar disc by the neutron star present in the systems, or is a function of their early (O9-B0) spectral type is as yet unclear (Clark et al. 1999).

4.3. Magnesium II *and Iron* II

Mg II and Fe II emission is observed in ∼30 per cent of the sample. Mg II emission is likely to be excited via Lyβ fluorescence (Bowen 1947), and is only seen in stars with spectral types earlier than B4. Assuming both Mg II transitions are optically thin, we would expect a flux ratio of Mg II 2.138:2.144 μm of ∼2.0 due to the greater statistical weight of the $5P_{3/2}$ level (and the same is true if the upper levels are populated via collisional excitation). Comparison of the line ratios in the 14 stars showing Mg II emission (and for which an EW is measurable) shows that $EW_{2.138} > EW_{2.141}$ for 10 stars with an average line ratio of Mg II 2.138:2.144 μm $\sim$ 1.9 i.e. close to the predicted value for optically thin emission.

Fe II emission is characteristic of moderately warm and dense environments ($T \sim 5000$ K, $N_e \geq 10^9$ cm^{-3}; Hamann & Simon 1987), both of which are expected to be satisfied in the circumstellar discs of Be stars. Comparison of the EW of the Fe II and Mg II transitions to Brγ indicates that while there is no direct correlation between the respective transitions, neither Fe II or Mg II emission is seen in stars with $EW_{Br\gamma} < 8$ Å.

4.4. Sodium I

Two Na I transitions exist at 2.206 & 2.209 μm. CD-27 11872 has 2 distinct features at these wavelengths that we attribute to Na I emission. Na I emission has previously only been identified in one Be star, HD 34921, the proposed optical counterpart of the X-ray source 1H0521 +37 (Polcaro et al. 1990; Clark et al. 1999 and references

therein); we note that CD-27 11872 has been proposed as a candidate Be/X–ray binary by Motch et al. (1997). An echelle spectrum of HD 34921 reveals two narrow (projected velocity < 50 km s^{-1}) emission features suggesting emission at large radii (assuming the lines arise in a Keplerian disc; Clark et al. 1999). Given the low ionisation energy (5.1 eV) of Sodium we might expect it to be fully ionised in the discs of Be stars; the presence of emission features suggests that a region(s) of the circumstellar envelope must be shielded from direct stellar radiation. IRAS $12-60$ μm fluxes for HD 34921 suggest the presence of cool dust, which could possibly shield the emitting regions in HD 34921 in a manner analogous to B[e] stars. Alternatively, changes in the disc geometry at large radii could produce large enough optical depths to shield the emitting regions from direct stellar radiation.

We find broad emission features at the correct wavelength for Na I emission in 3 stars; BD 12 5132 (BN0.2III), BD+5 3704 (B2.5V) and BD+29 4453 (B1.5V). The apparent width of these features implies a large projected velocity for the emitting regions of the circumstellar envelopes. If we assume that the requirements for the presence of Na I emission (i.e. shielding from direct stellar radiation) can only be fulfilled at large radii where sufficient material exists to prevent ionisation this suggests a radial acceleration of material at such distances. Clearly higher resolution spectra of this region are required before definitive conclusions can be made as to the presence and kinematics of possible Na I emitting regions in the envelopes of these stars.

5. Relations between emission line strengths and rotational velocity

Briot (1986) searched for a correlation between projected rotational velocity and emission characteristics for a large sample of Be stars, dividing early (B0-B5) stars into 2 classes showing strong (Fe II emission, strong IR excess) and weak (absence of Fe II emission, little or no IR excess) emission characteristics. It was found that the Be stars showing strong emission characteristics had a larger mean $v \sin i$ than the group of weak Be stars. Late (B6-B9) stars were found to have a mean $v \sin i$ comparable to the strongly emitting early stars. Briot (1986) interpreted this as suggesting that only hot, rapidly rotating stars can develop strong emission characteristics.

We characterised stars of spectral type B0-B4 as either strong or weak emitters based on the presence of Fe II emission (in practice a division at $\mathrm{EW}_{\mathrm{Br}\gamma} = 8$ Å; Sect. 4.3). The division into early and late stars at B4 was made based on the finding that neither Mg II or He I emission was seen in any star of a later spectral type. A further group comprising of stars with no evidence of emission (essentially appearing to be normal B stars – Sect. 4.1) was also defined ("non-e" stars). As we noted in Sect. 4.1 these may be misclassified B stars, or Be stars which are currently in a non-emission phase. In that section we showed that a comparison of the spectral class distribution of the "non-e" and "e" stars indicates that they appear to be from different populations.

Table 9. Mean breakup velocities of the subsets of the sample based on emission characteristics

	$\omega \sin i$
B0−B4(EW $>$ 8 Å) "e"	0.42 ± 0.03
B0−B4(EW $<$ 8 Å) "e"	0.37 ± 0.03
B5−B9 "e"	0.42 ± 0.04
B0−B9 "non-e" (groups 2&4)	0.21 ± 0.04

We choose to express the projected rotational velocities in terms of the critical breakup velocity of the individual star, v_{crit}, such that $\omega \sin i = v \sin i / v_{\mathrm{crit}}$. The critical breakup velocity was calculated according to Porter (1996)

$$v_{\mathrm{crit}} = \sqrt{0.67 \times GM/R} \quad (1)$$

where M and R are the stellar mass and radius taken from Schmidt-Kaler (1982).

The results of the analysis can be found in Table 9. Unlike Briot (1986) we find no *statistically significant* difference in mean $\omega \sin i$ between the strong and weak emitters. Likewise, no difference between the projected breakup velocities of the early and late stars is observed, in this case agreeing with the result of Briot (1986). However, the mean $\omega sini$ of the "non-e" stars *is* found to be lower than those of the "e" stars at the 4σ level. Two explanations are possible for this result. Firstly, the historical identification of the stars we identify as normal ("non-e") B stars as Be stars may have been incorrect; consequently we are simply observing the result that Be stars rotate more rapidly than B stars (e.g. Slettebak 1966). Alternatively, since a relationship between rotational velocity and the Be phenomenon clearly exists, *stars with lower rotational velocities may be more prone to phase changes between B and Be states*. The result that the B ("non-e") and Be ("e") stars are from different populations can then be explained by the result of Briot (1986) that there are no slowly rotating late Be stars, so the slowly rotating Be stars that have undergone a phase change and now appear as normal ("non-e") B stars should preferentially be of an early spectral type. This is the distribution found in Sect. 4.1 for the "non-e" objects. Future monitoring of the sample to see if the "non-e" objects undergo a phase transition back to "e", and hence truly are Be stars, will be necessary to differentiate between the two cases.

Table 4. Summary of emission features of Group 1 stars; equivalent widths are given in Å, where a *positive* EW corresponds to *emission*. *em* reflects emission in the relevant transition that is to weak to measure (typically < 0.2 Å), the addition of a question mark represents an uncertainty as to its presence. The estimated error in the equivalent widths is 20% unless marked with a colon (:) when it is 50%

Object	He I	Fe II	He I	Mg II	Mg II	He I	Brγ	Na I
name	2.058	2.089	2.113	2.138	2.144	2.161	2.166	2.206/9
CD−28 14778	3.4	0	0	1.4	0.9	em	24.0	0
CD−27 11872	4.5	0	0	1.2	0.7	em	12.7	em
BD−13 893	8.7	0	0	0	0	0	6.1	0
BD−12 5132	4.3	0	0	em	em	em?	7.2	em
BD−1 3834	0.9	0	−0.4	0.7	0.5	0	10.5	0
BD+1 1005	8.8:	0	0	0	0	em?	5.2	0
BD+4 1002	3.2	0	−0.9	0	0	0	1.2	0
BD+5 3704	0	0	−1.5	0	0	0	1.0:	em
BD+29 4453	1.1	0.5	0	0.8	0.7	0	16.9	em
BD+31 4018	1.6	0	0	0	0	0	9.2	0
BD+36 3946	3.9	0	0	0	0	0	5.8	0
BD+40 1213	1.5	0	0	0.5	0	0	21.0	0
BD+42 1376	0.5:	0	−0.6	0	0	0	1.8:	0
BD+45 3879	3.2	0.2	0	0.8	0.8	0	10.6	0
BD+47 3985	2.2:	0	−1.1	0.8	0.8	0	8.9	0
BD+55 605	8.5	0	1.3	0.3	0	em	8.6	0
BD+55 552	−1.9	0	0	0	0	0	1.6	0
BD+56 469	1.0:	0	−1.6	0	0	0	1.3	0
BD+56 473	2.0:	0	0	1.0:	0.4	0	4.2	0
BD+56 478	9.0	0.1	0	0	0	em?	8.7	0
BD+56 484	3.5	0.8:	0	0.9	0	0	16.9	0
BD+56 511	−0.5:	0	−0.9	0	0	0	3.7:	0
BD+56 573	0.8:	1.0:	0	0.9	0	0	15.4	0
BD+57 681	6.7:	0	1.2:	0	0	0	4.6	0
BD+58 2320	3.4	0	0	0	0	0	7.2	0

Table 5. Summary of emission features of Group 2 stars. See Table 4 for explanation

Object	He I	Fe II	He I	Mg II	Mg II	Brγ
name	2.058	2.089	2.112	2.138	2.144	2.166
CD −25 12642	0	0	−1.3	0	0	−3.9
BD+20 4449	0	0	−1.1	0	0	−5.0
BD+23 1148	0	0	−1.2	0	0	−4.0
BD+25 4083	0	0	−1.5	0	0	−4.1
BD+27 797	em	0	0	0	0	−6.5
BD+27 850	0	0	−1.2	0	0	−7.3
BD+28 3598	−0.8	0	−1.2	0	0	−2.7
BD+29 3842	0.9	0	−1.5	0	0	−3.3
BD+37 3856	0	0	−1.2	0	0	−6.2
BD+45 933	0	0	−1.0	0	0	−5.4
BD+56 493	0	0	−1.1	0	0	−5.5

Table 6. Summary of emission features of Group 3 stars. See Table 4 for explanation

Object	He I	Fe II	He I	Mg II	Mg II	Brγ
name	2.058	2.089	2.112	2.138	2.144	2.166
BD−8 929	0	0	0	em	em	8.1
BD+42 4538	0	0.8	0	0.1:	0.6	21.7
BD+47 183	0	0.3	0	0.5	0.3	17.7
BD+47 857	0	1.4	0	em	em	17.0
BD+47 939	0	0.2	0	0.3	0.6	13.6

Table 7. Summary of emission features of Group 4 stars. See Table 4 for explanation

Object name	He I 2.058	Fe II 2.089	He I 2.112	Mg II 2.138	Mg II 2.144	Brγ 2.166
BD−19 5036	0	0	0	0	0	−6.9
BD+17 4087	0	0	0	0	0	−6.1
BD+19 578	0	0	0	0	0	−4.3
BD+27 797	0	0	0	0	0	−6.5
BD+30 3227	0	0	0	0	0	−4.8

Table 8. Summary of emission features of Group 5 stars. See Table 4 for explanation

Object name	He I 2.058	Fe II 2.089	He I 2.112	Mg II 2.138	Mg II 2.144	Brγ 2.166
CD−27 16010	0	0	0	0	0	−3.4
CD−27 13183	0	0	0	0	0	0.1
BD−20 5381	0	0	0	0	0	9.3
BD−5 1710	0	0	0	0	0	3.4
BD−2 5328	0	0	0	0	0	2.9
BD−0 3543	0	0	0	0	0	0.7
BD−0 1468	0	0.8	0	0	0	8.7
BD+0 1203	0	0	0	0	0	7.1
BD+2 3815	0	0.4	0	0	0	4.6
BD+21 4695	0	0.4	0	0	0	−2.4
BD+27 3411	0	0	0	0	0	−1.8
BD+37 675	0	0.9:	0	0	0	6.8
BD+43 1048	0	0	0	0	0	3.3
BD+46 275	0	0	0	0	0	−1.4
BD+49 614	0	0.2	0	0	0	2.5
BD+50 825	0	0	0	0	0	3.3
BD+50 3430	0	0	0	0	0	3.8
BD+51 3091	0	0	0	0	0	−4.2
BD+53 2599	0	0	0	0	0	−1.9
BD+55 2411	0	0	0	0	0	−3.1
BD+58 554	0	0	0	0	0	6.5

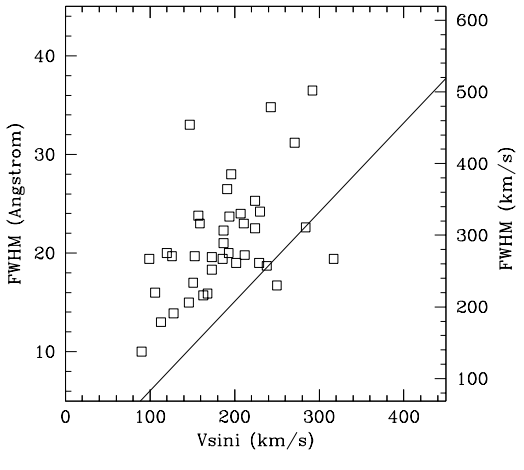

Fig. 5. Plot of Brγ $FWHM$ against projected rotational velocity. Solid line indicates $FWHM = v \sin i$

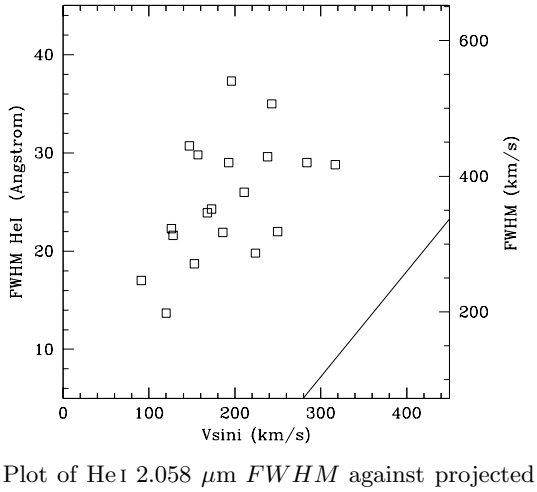

Fig. 6. Plot of He I 2.058 μm $FWHM$ against projected rotational velocity. Solid line indicates $FWHM = v \sin i$

6. Line profile morphology

6.1. General line profile morphology

A number of different line profiles are observed in our data set; at the resolution of our observations these are all seen to have counterparts in optical spectra (single & double peaked profiles and shell lines). Waters & Marlborough (1994) present high resolution and S/N spectra of the Brγ

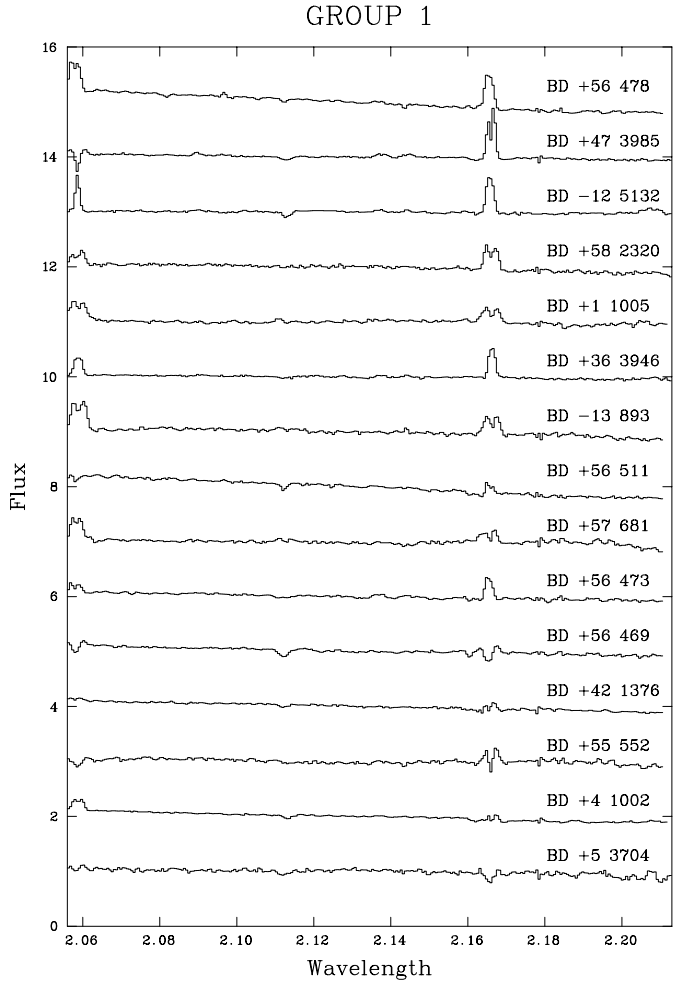

Fig. 7. Stars belonging to Group 1: I. Wavelength given in microns, flux normalised and with offset applied

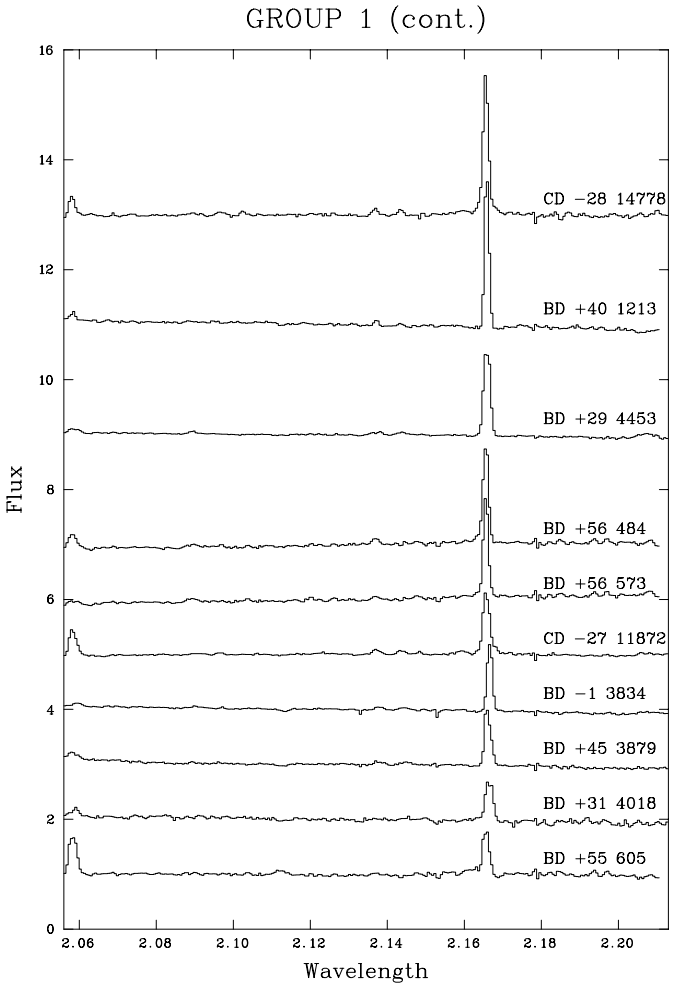

Fig. 8. Stars belonging to Group 1: II. Wavelength given in microns, flux normalised and with offset applied

transition of ψ Per and 59 Cyg, and find the line profiles have no counterparts in the optical spectra; unfortunately our spectra are of insufficient resolution for us to search for such profiles, although we note that the broad, flat topped He I 2.058 μm features in BD+4 1002 & BD+29 4453 (Figs. 7 and 8) superficially resemble the Brγ profile of 59 Cyg at the resolution of our spectra.

Of the sample of 66 isolated Be stars, 40 show Brγ in emission and 3 show shell profiles. Of these stars BD+47 3985 clearly shows the effects of differing optical depths in the He I 2.058 μm and Brγ lines, with He I 2.058 μm having a pronounced shell profile (indicating a large optical depth) while the central absorption in Brγ does not extend below the level of the continuum.

Systematic changes in line profile with spectral type are only seen in Brγ, with the emission component seen superimposed on a photospheric absorption component in the spectra of late (B7-B9) stars. Given the late spectral type (and hence relatively low temperatures of these stars) this is unlikely to be a NLTE effect of the type identified by Murdoch et al. (1994). Rather it is likely to be due to a combination of the increasing strength of the photospheric feature and a reduction in the strength of emission due to the reasons outlined in Sect. 4.1. Additionally, the interplay of line source functions and opacities with stellar (and hence disc) temperature produces intrinsically narrower profiles for the cooler stars. For disc temperatures of 10 000 K and 6 000 K the line source function, S, throughout the disc is lower for the cooler disc than the hotter disc. However, close to the star (within $\sim$1 R_*) the disc opacity, κ, is also *lower* for the cooler disc than the hotter disc, while at larger radii the opacity of the cooler disc is *larger* than that of the hotter disc. Consequently the emission from the innermost part of the disc increases relative to the outer disc, and since the inner region is rapidly rotating (assuming a Keplerian disc) an increase in emission in the high velocity line wings is seen. However, for discs with temperatures lower than 6 000 K there is no such region where $\kappa_L/\kappa_H < S_L/S_H$ (where the suffixes L and H refer to lower and higher temperature discs respectively) ie the decrease in the source function with lower temperatures is always *greater* than the change in opacity *throughout the*

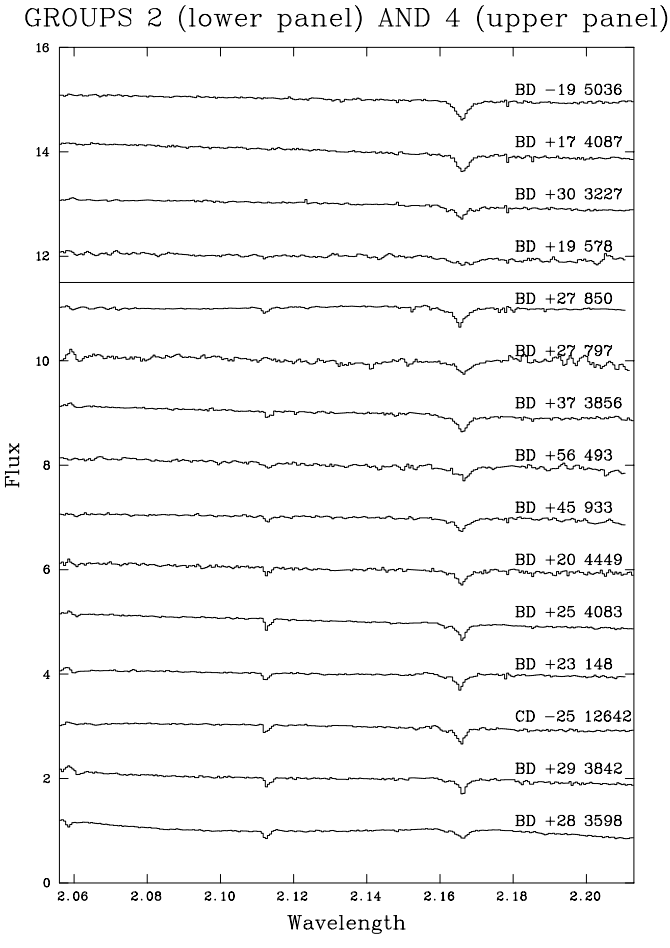

Fig. 9. Stars belonging to Groups 2 & 4. Wavelength given in microns, flux normalised and with offset applied

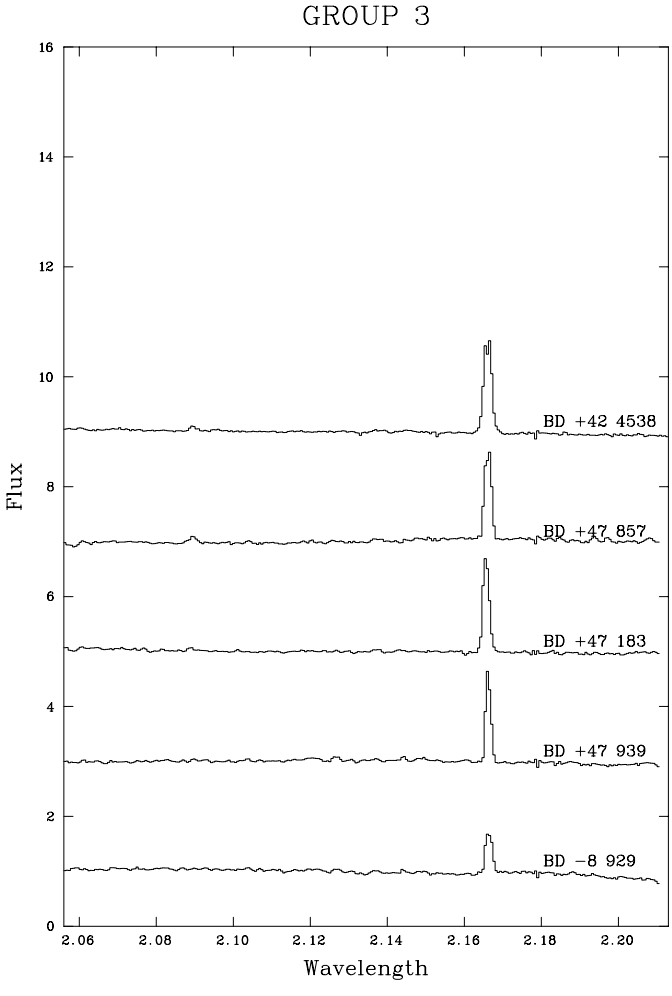

Fig. 10. Stars belonging to Group 3. Wavelength given in microns, flux normalised and with offset applied

entire disc. This means that in addition to a reduction in the source function, radiation finds it more difficult to escape from the rapidly rotating innermost regions of the disc, and so there is less emission in the high velocity wings of the IR lines, and so they appear narrower. Combined with the greater strength of the underlying photospheric feature in the cooler stars this means that narrow emission lines superimposed on strong photospheric absorption features are favoured, which is observed.

6.2. Line widths & projected rotational velocity

Several workers have investigated the relationships between line widths, equivalent widths and projected stellar rotational velocity (e.g. Dachs et al. 1986; Hanuschik 1989). They find evidence for a positive correlation between the projected stellar rotational velocity and the full width half maximum ($FWHM$) of the optical H I and Fe II lines. A further, weaker anti correlation was also found between the EW and $FWHM$ of the lines. These relations are indicative of rotational broadening in the circumstellar material, where the lines with greater EW and smaller $FWHM$ arise from disc regions with a greater radial extent (and hence lower rotational velocity).

We measured the $FWHM$ of the Brγ and He I 2.058 μm profiles, and plotted these against the projected rotational velocities of the stars. (Figs. 5 and 6). A correlation between the $FWHM$ of Brγ and (weakly) He I 2.058 μm, and v sin i is observed, with a "conical" distribution of points which is a characteristic of the plots of Hanuschik (1989). Best fits to the data give

$$FWHM(\mathrm{Br}\gamma) = 0.759\ v \sin i + 149 \text{ km s}^{-1} \quad (2)$$

and

$$FWHM(\mathrm{He\ I}) = 0.643\ v \sin i + 247 \text{ km s}^{-1}. \quad (3)$$

We note that with the exception of 2 stars in the Brγ plot, all the points are found to lie above a line corresponding to $FWHM = v \sin i$.

No inverse correlation between EW and v sin i was found in either the Brγ or He I data sets. This is likely to be due to the relatively large scatter observed in the EW datasets, given that the relationship is rather weak in the Hα dataset of Hanuschik (1989).

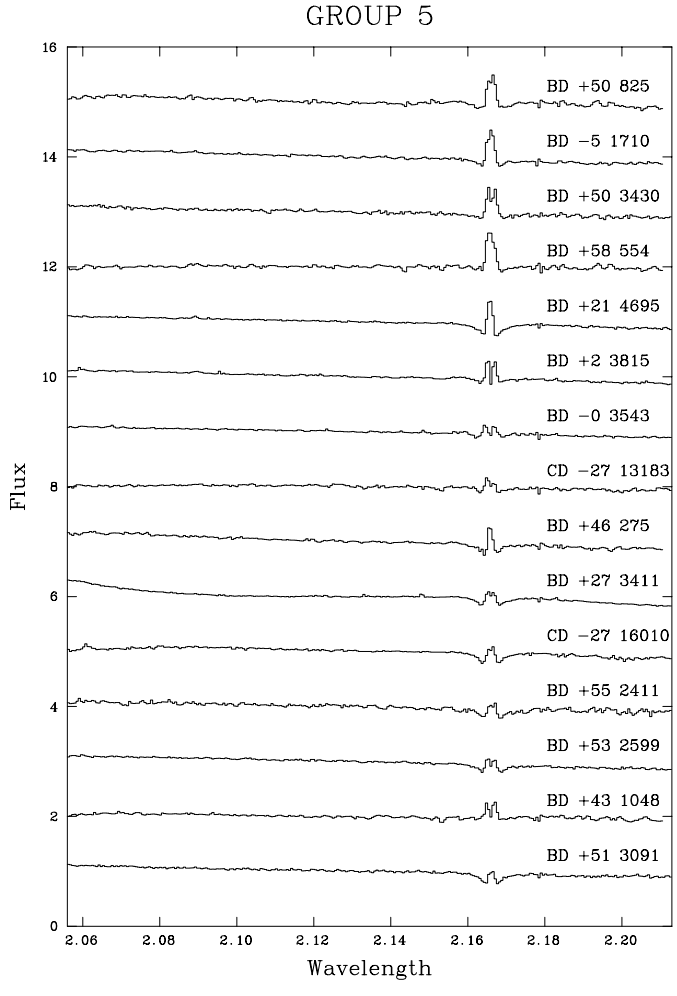

Fig. 11. Stars belonging to Group 5: I. Wavelength given in microns, flux normalised and with offset applied

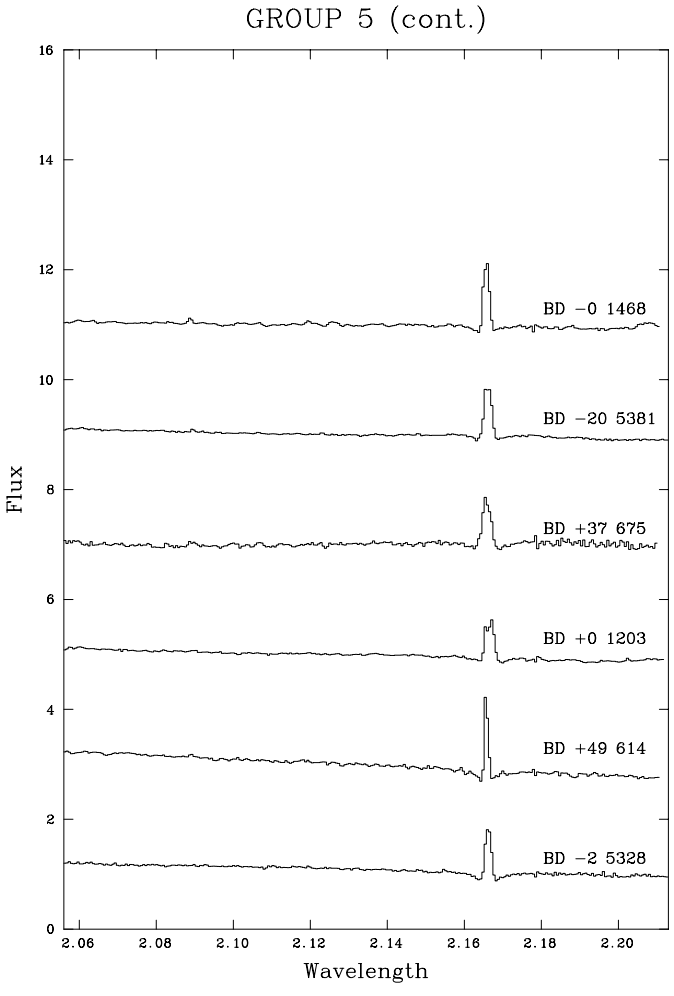

Fig. 12. Stars belonging to Group 5: II. Wavelength given in microns, flux normalised and with offset applied

6.3. V/R asymmetry

Many Be stars show asymmetric profiles, which exhibit a cyclic V(iolet)/R(ed) variability with periods ranging from $1-10$ years, due to a one armed density wave in the circumstellar envelope (e.g. Okazaki 1991, 1997). We find that a total of 21 stars show double peaked profiles, with a subset of 5 showing asymmetric profiles.

One star, BD+58 2320, shows double peaked asymmetric line profiles in He I 2.058 μm and Brγ, but with opposite V/R ratios (Fig. 7). An interpretation of the line profiles based on differences in the radial velocities of the emitting regions is unlikely given that the Hα line profiles show little evidence for large velocities over the regions of the disc responsible for optical and IR Hydrogen line emission. One possible explanation would be the presence of an inhomogeneous circumstellar environment, possibly as a result of discrete mass ejection events as envisaged for μ Cen (e.g. Hanuschik et al. 1993). This would suggest that rapid variability should be seen in the line profiles as the circumstellar material is circularised via viscous redistribution of angular momentum. Another possibility is that the difference in V/R ratio between lines arising at different radii (where He I emission forms at larger radii than Brγ) reflects the presence of a spiral density wave within the circumstellar disc. Such an explanation would suggest slow, correlated evolution of the V/R ratio for the two lines, and a possible systematic change in ratio through the various Hydrogen series as higher transitions probe regions closer to the star, and thus experience different disc densities. Time resolved observations are required to differentiate between these two possibilities.

7. Conclusions

We have analysed the spectra of 66 isolated Be stars and found emission from H I, He I, Mg II, Fe II and Na I to be present in subsets of the spectra. We find the presence of He I and Mg II features to be a good diagnostic of early spectral type. The possible presence of Na I emission in the spectrum of 4 stars appears to indicate that regions of

the circumstellar envelopes of these stars must be shielded from direct stellar radiation.

Systematic trends in the line strength and profile of Brγ are seen from early to late spectral types; this can be understood in terms of differences in the disc temperature and density (and the increasing strength of the photospheric feature in the later stars). Correlations between the $FWHM$ of Brγ and He I 2.058 μm and the stellar rotational velocity were found. No correlations were found between stellar rotational velocity and the EW of either of these transitions.

No significant difference between the projected rotational velocities of the stars (expressed as a function of the stellar breakup velocity) and the emission characteristics (defined by the strength of Brγ emission and the presence of Mg II) of the emission line stars was found. However, stars which appear to have undergone a phase transition from emission ("e") to non emission ("non-e") stars were found to have a smaller mean rotational velocity than the Be stars in the sample. In addition these objects have a distribution of spectral types that is significantly earlier than the emission line objects. This can be explained either as the original misidentification of these objects as Be stars (i.e. they never had line emission), or as evidence that stars with low rotational velocities may be more prone to changes between the Be and B phases.

Acknowledgements. We wish to thank the UK PATT panel for the allocation of observing time for this programme. In addition we thank the support astronomers and staff of UKIRT for their invaluable assistance at the telescope, and Ignacio Negueruela for his valuable input. UKIRT is operated by the Joint Astronomy Centre, Hawaii for the UK PPARC. Data reduction and analysis for this paper was carried out using the Liverpool JMU and Sussex University Starlink Nodes. JSC wishes to acknowledge a PPARC research award.

References

Bowen I.S., 1947, PASP 59, 196
Briot D., 1986, A&A 163, 67
Clark J.S., Steele I.A., Fender R.P., Coe M.J., 1999, A&A 348, 888
Dachs J., Hanuschik R.W., Kaiser D., Rohe D., 1986, A&A 159, 276
Hamann F., Simon M., 1987, ApJ 318, 356
Hanson M.M., Conti P.S., Rieke M.J., 1996, ApJS 107, 281 (HCR96)
Hanuschik R.W., 1989, Astron. Space Sci. 161, 61
Hanuschik R.W., Dachs J., Baudzus M., Thimm G., 1993, A&A 274, 356
van Kerkwijk M., Waters L., Marlborough J., 1995, A&A 300, 259
Marlborough J.M., Zijlstra J.-W., Waters L.B.F.M., 1997, A&A 321, 867 (MZW97)
McGregor P.J., Hyland A.R., Hillier D., 1988, ApJ 324, 1071
Morris P.W., Eenens P.R.J., Hanson M.M., Conti P.S., Blum R.D., 1996, ApJ 470, 597
Motch C., Haberl F., Dennerl K., Pakull M., Janot-Pacheco E., 1997, A&A 323, 853
Murdoch K.A., Drew J.E., Anderson L.S., 1994, MNRAS 284, L27
Okazaki A.T., 1991, PASJ 43, 75
Okazaki A.T., 1997, A&A 318, 548
Polcaro, et al., 1990, A&A 231, 354
Porter J.M., 1996, MNRAS 280, L31
Puxley P.J., Beard S.M., Ramsay S.K., 1992, in: Data Analysis Workshop-4th ESO/ST-ECF. Garching, p. 117
Quirrenbach A., Buscher D.F., Mozurkewich D., Hummel C.A., Armstrong J.T., 1994, A&A 283, 13
Schmidt-Kaler Th., 1982, in: Schaifers K., Voigt H.H. (eds.), Landolt Bornstein New Series, Vol. 2b. Springer-Verlag, Berlin
Slettebak A., 1966, ApJ 145, 121
Stee P., de Araujo F.X., Vakili F., et al., 1995, A&A 300, 219
Steele I.A., Negueruela I., Clark J.S., 1999, A&AS (submitted) (Paper I)
Walborn N.R., 1976, ApJ 205, 419
Waters L.B.F.M., 1986, A&A 162, 121
Waters L.B.F.M., Marlborough J.M., 1994, Balona L.A., Henrichs H.F., Le Contel J.M. (eds.), IAU Symp. 162, Pulsation, Rotation and Mass Loss in Early Type Stars. Kluwer, Dordrecht, p. 241
Zorec J., Briot D., 1997, A&A 318, 443